ACS Medicinal Chemistry Letters

pubs.acs.org/acsmedchemlett Letter

Spirocyclic Thiohydantoin Antagonists of F877L and Wild-Type Androgen Receptor for Castration-Resistant Prostate Cancer

Zhuming Zhang,* Peter J. Connolly, Luis Trabalón Escolar, Christian Rocaboy, Vineet Pande, Lieven Meerpoel, Heng-Keang Lim, Jonathan R. Branch, Janine Ondrus, Ian Hickson, Tammy L. Bush, James R. Bischoff, and Gilles Bignan*

Cite This: ACS Med. Chem. Lett. 2021, 12, 1245−1252 Read Online

ACCESS | Metrics & More | Article Recommendations | Supporting Information

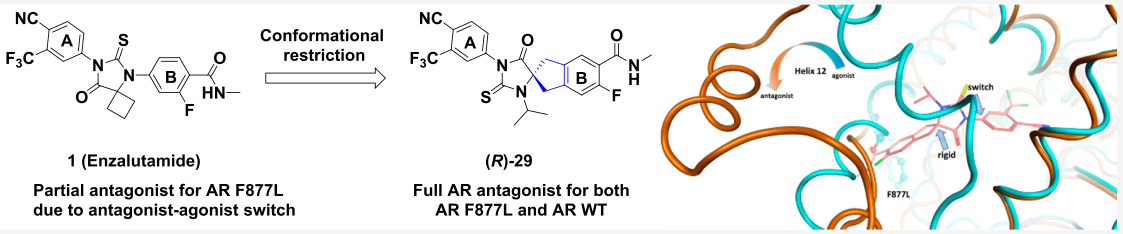

ABSTRACT: Androgen receptor (AR) transcriptional reactivation plays a key role in the development and progression of lethal castration-resistant prostate cancer (CRPC). Recurrent alterations in the AR enable persistent AR pathway signaling and drive resistance to the treatment of second-generation antiandrogens. AR F877L, a point mutation in the ligand binding domain of the AR, was identified in patients who acquired resistance to enzalutamide or apalutamide. In parallel to our previous structure−activity relationship (SAR) studies of compound **4** (JNJ-pan-AR) and clinical stage compound **5** (JNJ-63576253), we discovered additional AR antagonists that provide opportunities for future development. Here we report a highly potent series of spirocyclic thiohydantoins as AR antagonists for the treatment of the F877L mutant and wild-type CRPC.

KEYWORDS: *Androgen receptor, spirocyclic, thiohydantoin, resistance, apalutamide, LBD, prostate cancer*

Molecular profiling studies have shown that recurrent genomic alterations in the master regulator androgen receptor (AR) and its pathway is a common feature that drives resistance to the second-generation AR-targeted therapies abiraterone acetate, enzalutamide (**1**, Figure 1), and apalutamide (**3**, Figure 2) for the treatment of advanced prostate cancer.[1−5] AR transcriptional reactivation and persistent AR signaling are now understood as the central cores of resistance mechanisms in disease progression leading to lethal metastatic castration-resistant prostate cancer (mCRPC).[6,7] Sustained AR signaling in CRPC tumors has been reported to be the result of numerous genomic aberrations including well-documented gene alteration, amplification, overexpression, splice variant isoform expression (AR-V7), ligand binding domain (LBD) point mutations, and

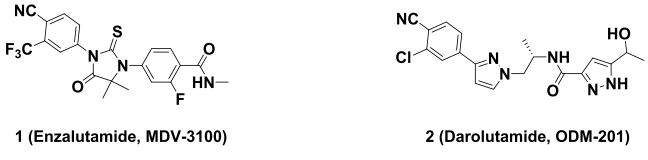

Figure 1. Chemical structures of enzalutamide (**1**) and darolutamide (**2**).

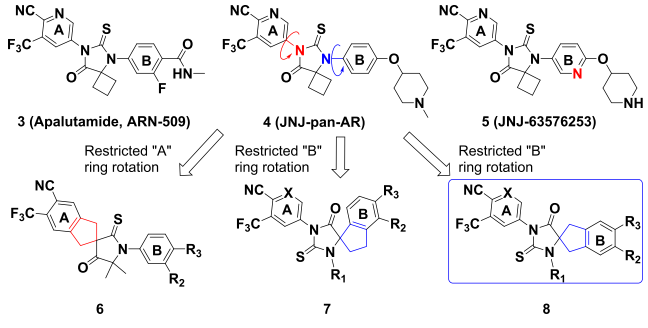

Figure 2. Chemical structures of **3** (apalutamide ARN-509), **4** (JNJ-pan-AR), **5** (JNJ-63576253), and bioisosteric spirocyclic scaffolds **6**, **7**, and **8** proposed as antagonists of the AR WT and AR F877L. Compound class **8** was the focus of our lead optimization efforts.

Received: January 18, 2021
Accepted: June 28, 2021
Published: June 29, 2021

https://doi.org/10.1021/acsmedchemlett.1c00032
ACS Med. Chem. Lett. 2021, 12, 1245−1252

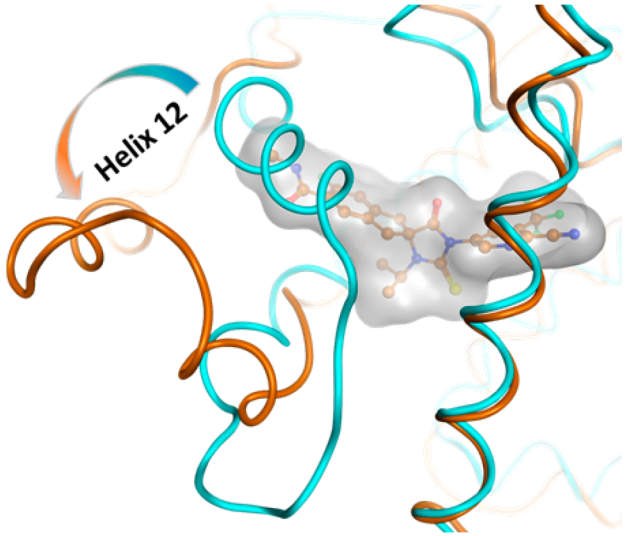

Figure 3. Manual docking model of (*R*)-**28** (orange balls and sticks with gray surface) bound to a potentially antagonistic conformation (orange tubes) of the AR LBD. Superposition of a crystal structure of the AR in a putative agonistic conformation is shown in cyan tubes (PDB ID: 1T5Z).

Table 1. Chemical Structures of Compounds 9−29

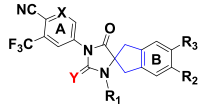

9-29

Compound	X	Y	R_1	R_2	R_3
9	N	S	H	H	
10	CH	S	H	H	
11	N	S	Me	H	
12	CH	S	Me	H	
13	N	S	Me	F	
14	CH	S	Me	F	
15	CH	O	Me	H	
16	N	S	Me	H	
17	N	S	Me	H	OH
18	N	S		F	
19	CH	S		F	
20	N	S		F	
21	CH	S		F	
22	N	S		F	
23	N	S		F	
24	N	S		F	
25	N	S		F	
(*S*)-26	N	S		F	
(*S*)-27	CH	S		F	
(*R*)-28	N	S		F	
(*R*)-29	CH	S		F	

Scheme 1. Synthesis of Spirocyclic Thiohydantoin Analogues 18−22 and 26−29[a]

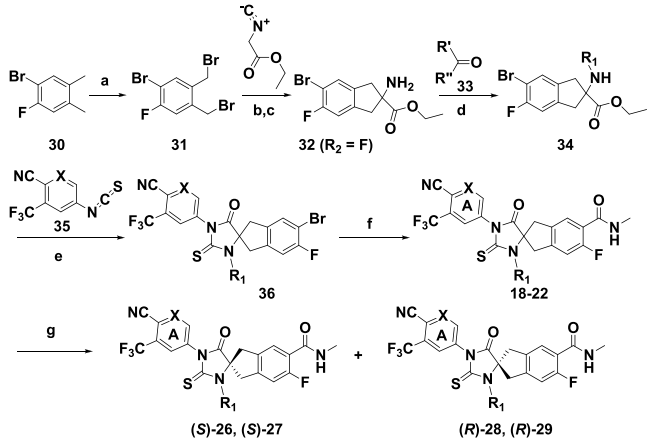

[a]Reagents and conditions: (a) NBS, AIBN (cat), CCl_4, 85 °C; (b) K_2CO_3, 18-*crown*-6, MeCN, rt; (c) aq. HCl, rt; (d) $NaBH(OAc)_3$, DCE, rt; (e) TEA, THF/DMF, 80 °C; (f) $MeNH_2$·HCl (or MeNHOMe·HCl), $W(CO)_6$ (cat.), $Pd(OAc)_2$ (cat.), Xantphos (cat.), TEA, 1,4-dioxane, 80 °C; (g) SFC chiral separation.

Scheme 2. Synthesis of Spirocyclic Thiohydantoin or Hydantoin Analogues 11−15[a]

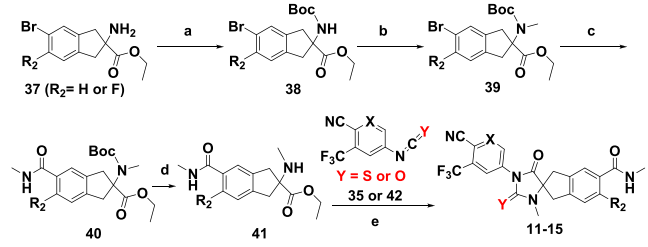

[a]Reagents and conditions: (a) Boc_2O, TEA, DCM, rt; (b) MeI, NaH, DMF, rt; (c) MeNHOMe·HCl, $W(CO)_6$ (cat.), $Pd(OAc)_2$ (cat.), Xantphos (cat.), DMAP, K_3PO_4, 1,4-dioxane, microwave, 120 °C; (d) TFA, DCM, rt; (e) TEA, THF, DMF, 80 °C.

Scheme 3. Synthesis of Spirocyclic Thiohydantoin Analogue 16 and Phenol Metabolite 17[a]

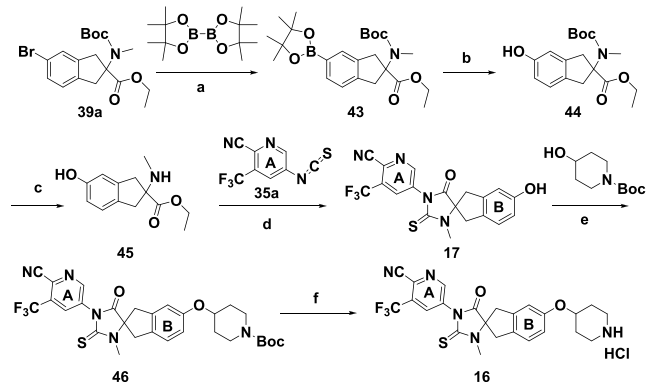

[a]Reagents and conditions: (a) $Pd(dppf)Cl_2$, KOAc, 1,4-dioxane, 80 °C; (b) oxone, acetone, rt; (c) TFA, DCM, rt; (d) TEA, THF, DMF, 80 °C; (e) DEAD, PPh_3, THF, 60 °C; (f) HCl, 1,4-dioxane, rt.

glucocorticoid receptor (GR) bypass.[1,8−12] Colloquially dubbed as "A Resilient Foe", retargeting the AR by molecularly targeted therapy with a precision medicine approach still

https://doi.org/10.1021/acsmedchemlett.1c00032
ACS Med. Chem. Lett. 2021, 12, 1245−1252

Scheme 4. Synthesis of Spirocyclic Thiohydantoin Analogues 23−25[a]

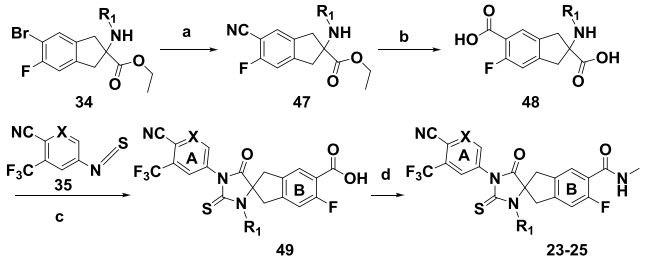

[a]Reagents and conditions: (a) $Zn(CN)_2$, Pd_2dba_3, PPh_3, DMA, 120 °C; (b) aqueous conc. HCl, 135 °C; (c) TEA, THF/DMF, 80 °C; (d) NH_4Cl, HBTU, DIPEA, DMAP (cat.), DMF, rt.

Table 2. Transcriptional Reporter Assay Activity of 9−16 and 19−29 in LNCaP F877L (Mutant) and LNCaP AR cs (WT) Cells

compound	LNCaP F877L[a] IC_{50} (nM)[b]	LNCaP WT[a] IC_{50} (nM)[b]
1	not fit	117 ± 66
4	98 ± 63	191 ± 120
9	>15000[c]	>15000[d]
10	5012 ± 207	11220 ± 3826[e]
11	676 ± 170	1380 ± 141
12	525 ± 322	646 ± 113
13	759 ± 81	1096 ± 7
14	339 ± 119	398 ± 52
15	1660 ± 1081	>30000
16	178 ± 86	219 ± 116
18	145 ± 32	112 ± 28
19	93 ± 32	93 ± 30
20	102 ± 10	100 ± 20
21	123 ± 39	126 ± 8
22	257 ± 13	191 ± 11
23	170 ± 37	229 ± 25
24	132 ± 33	148 ± 39
25	174 ± 4	209 ± 6
(*S*)-**26**	112 ± 116	178 ± 41
(*S*)-**27**	151 ± 26	170 ± 19
(*R*)-**28**	65 ± 47	52 ± 37
(*R*)-**29**	78 ± 10	72 ± 23

[a]LNCaP F877L and LNCaP WT reporter assays were repeated two times or more. All compounds except **1** were antagonists in AR F877L, and all were antagonists in the AR WT. [b]Max inhibition >90% for all compounds unless specifically mentioned. [c]Max inhibition 52%. [d]Max inhibition 35%. [e]Max inhibition 80%.

represents a major therapeutic opportunity for the treatment of mCRPC.[13]

The AR belongs to the steroid hormone group of nuclear receptors that includes the estrogen receptor (ER), GR, and progesterone receptor (PR), and it functions as a ligand-inducible transcription factor that is activated by the binding of androgens such as testosterone and dihydrotestosterone (DHT) to its LBD.[14] Point mutations in the AR LBD have been associated with 10−20% of the resistance that converts antagonists into agonists upon ligand binding, driving the disease through the reactivation of AR signaling.[15] For example, the missense mutation of phenylalanine to leucine at AR amino acid 877 (F877L, formerly known as F876L) was reported in 2013 to confer resistance to both enzalutamide and apalutamide, leading to an antagonist-to-agonist switch.[10,11]

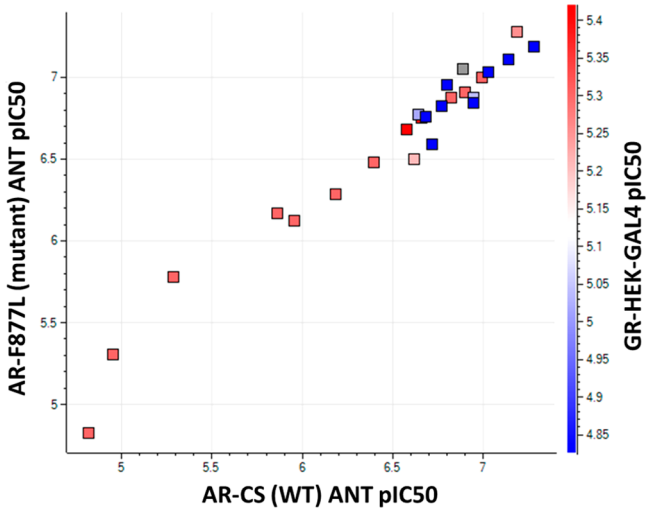

Figure 4. Correlation between AR F877L (*y* axis) and the AR WT (*x* axis) antagonistic pIC50 and the AR WT pIC50 in transporter assays along with the GR antagonistic pIC50 (red−blue color scale).

AR F877L was found to occur spontaneously in cells after prolonged treatment with enzalutamide and apalutamide. AR F877L was also detected in the plasma circulating tumor DNA (ctDNA) for 3 of 29 progressing patients enrolled in the apalutamide Phase I clinical trial.[15] Recently, the next-generation AR antagonist darolutamide (ODM-201, **2**, Figure 1) was reported to overcome resistance mechanisms including AR F877L mutation and was subsequently approved for nonmetastatic castration-resistant prostate cancer (nmCRPC) by the U.S. Food and Drug Administration (FDA).[16]

Recently, we published our work on the characterization and optimization of compound **4** (JNJ-pan-AR). focusing on the substituents of ring "A" as well as ring "B" and its periphery, leading to the discovery of the clinical stage compound **5** (JNJ-63576253).[17] In our putative AR homology model, the mechanism for the antagonist-to-agonist switch of enzalutamide (**1**) or apalutamide (**3**) in the AR F877L mutant tumors could be explained by comparing the open ("antagonistic") and closed ("agonistic") conformations, respectively, of Helix 12 located in the LBD.[17−20]

To complement our reported work on rings "A" and "B" of compound **4**, we decided to expand our exploration of the hydantoin core by investigating additional spirocyclic compound classes such as scaffolds **6**, **7**, and **8** in an effort to preserve the key structural features of the pharmacophore, reduce the ligand conformational flexibility, and improve the suboptimal pharmacological parameters of compound **4**. Here we report our work on the discovery of a series of spirocyclic thiohydantoins based on scaffold **8** that are highly potent antagonists of the AR WT and AR F877L (Figure 2).

Our early models of bicalutamide, enzalutamide (**1**), and apalutamide (**3**) suggested that reducing the flexibility within this class of ligands by conformational restriction would have an impact on the antagonist-to-agonist switch in AR F877L without the need for peripheral bulky substituents (Supplementary Section S-12).[21,23,24] To test this hypothesis (Figure 3, Supplementary Section S-12), we designed rigidified scaffolds **6**, **7**, and **8** with a spirocyclic central core to add rotational restriction in thiohydantoin series (Figure 2). The concept of conformation restriction by the cyclization of an acyclic group via a bioisosteric spirocyclic ring has emerged as

https://doi.org/10.1021/acsmedchemlett.1c00032
ACS Med. Chem. Lett. 2021, 12, 1245−1252

Table 3. Antiproliferative Activity of 12, 16, 18−20, and 26−29 in the VCaP Prostate Cancer Cell Line Compared with That of 1 and 4[a]

compound	1	4	12	16	18	19	20	(*S*)-26	(*S*)-27	(*R*)-28	(*R*)-29
VCaP IC_{50} (nM)	149 ± 30	92 ± 71	2440 ± 2010	40 ± 40	30 ± 20	50 ± 20	10 ± 10	680 ± 150	480 ± 50	40 ± 10	110 ± 30

[a]VCaP cells (WT AR) were cultured in the presence of 30 pM R1881, and the extent of androgen-dependent proliferation was calculated. The VCaP antiproliferative assay was repeated two times or more.

Table 4. Human Liver Microsomal (HLM) $T_{1/2}$, Permeability, and Mean Single-Dose PK Parameters of Compounds 16, 18, 19, and 26−29 in CD-1 Male Mice by PO and IV Dosing

compound	16	18	19	(*S*)-26	(*S*)-27	(*R*)-28	(*R*)-29
HLM_$T_{1/2}$ (min)[a]	>180	>180	>180	118	>180	135	>180
P_{app} A > B (+inh.) (cm/s × 10^{-6})[c]	6.4	36.5	35.2	35.5	24.4	16.6	34.5
PO dose (mg/kg)	10	10	10	10	10	10	10
$AUC_{0\text{-inf}}$ (μg·h/mL)	15.2	27.0	107	39.1	50.4	99.4	104
C_{max} (μM)	0.92	3.69	8.85	3.7	5.81	6.1	5.86
IV dose (mg/kg)	2	2	2	2	2	2	2
CL (mL/min/kg)	11.5	3.4	1.6	4.0	3.0	1.3	0.9
$T_{1/2}$ (h)	16.7	19.5	14.8	6.9	5.2	15.8	10.3
Vdss (L/kg)	16.3	4.8	1.7	2.3	1.8	1.9	1.7
F (%)[b]	97	61	102	92	91	80	63

[a]For HLM $T_{1/2}$: high stability >180 min; 33 min < medium stability <180 min; low stability < 33 min. [b]Oral bioavailability. [c]Passive permeability was measured from the apical (A) to the basolateral side (B) of the MDCK-MDR1 cells in the presence of a P-glycoprotein (P-gp) inhibitor.

an effective approach in drug discovery in the past decade.[22] Initially, we explored the structure−activity relationship (SAR) for compounds in classes **6** and **7**, but unfortunately, either significant a loss of potency (**6**) or a surprising enhanced intrinsic agonism (**7**) rendered these compounds difficult to progress (data not shown). Thus we focused on scaffold **8** while simultaneously taking advantage of the insight gained from the development of **5** (JNJ-63576253).

In contrast with our previous SAR studies, our exploration of scaffold **8** preserved the key pharmacophore elements of peripheral rings "A" and "B" in **1** (enzalutamide), **3** (apalutamide), and **4** (JNJ-pan-AR) to better understand the impact of the central spirocyclic core alteration, as shown in analogues **9**−**29** (Table 1). For example, compound **16** preserved two key features of **4**: a piperidinyl group on ring "B" and an identical "A" ring. Similarly, compounds **14**, **19**, and (*R*)-**29** kept the same "A" and "B" rings as **1**.

The general syntheses of analogues **9**−**16**, **18**−**29**, and metabolite **17** are outlined in Schemes 1−4. In Scheme 1, substituted 2-aminoindan-2-carboxylic ester **32** was prepared starting from **30** following literature procedures.[25,26] Reductive alkylation reactions of **32** with an aldehyde such as isobutyraldehyde or a ketone such as acetone, cyclobutanone, cyclopentanone, or cyclohexanone in the presence of sodium triacetoxyborohydride provided *N*-alkylated **34**, which was then cyclized to **36** by heating with isothiocyanate **35**. The Pd-catalyzed Heck aminocarbonylation of **36** using $W(CO)_6$ provided racemic analogues **18**−**22**.[27] The chiral supercritical fluid chromatography (SFC) separation of **18** and **19** led to the corresponding chirally pure (*S*)-**26**, (*S*)-**27** and (*R*)-**28**, (*R*)-**29**. Because we were unable to obtain crystal structure of these molecules, the assignments of the absolute stereochemistry for **26**−**29** were based on vibrational circular dichroism (VCD) experiments (Supplementary Sections S-8 and S-9). Confirmation of these assignments by unambiguous asymmetric synthesis was beyond the scope of this program.

In Scheme 2, commercially available or synthetically readily accessible **37** (R_2 = H or F) or synthetically readily accessible **32** (R_2 = F) was protected with a Boc group to give **38**.[25,26] The *N*-methylation of **38** with iodomethane and sodium hydride followed by Pd-catalyzed Heck aminocarbonylation of **39** using $W(CO)_6$ and the subsequent removal of the Boc group provided **41**, which was cyclized with isothiocyanate **35** or isocyanate **42** to analogues **11**−**15**. Analogues **11**−**15** could also be prepared by the Boc deprotection of **39** and elaboration following the methods previously described in Scheme 1. Compounds **9** and **10** were prepared from **38** by the procedures described in Scheme 2 but omitting *N*-methylation (step b) (Supplementary Section S-7).

In Scheme 3, phenol **44** was obtained by converting aryl bromide **39a** to boronic ester **43** followed by oxidative cleavage. The subsequent removal of the Boc group and the cyclization of **45** with isothiocyanate **35** led to intermediate **17**, which was then converted to analogue **16** by the Mitsunobu reaction and subsequent treatment with HCl. In Scheme 4, the palladium-catalyzed cyanation of aryl bromide **34** using $Zn(CN)_2$ under mild conditions afforded nitrile **47**, which was hydrolyzed to diacid **48** and subsequently cyclized to **49** without isolation by heating with isothiocyanate **35**. By comparison with the route illustrated in Scheme 1, this route offered several advantages. The final step involving a flexible amide coupling reaction not only provided diversified "B"-ring carboxamide derivatives but also avoided potential contamination of the final product with palladium, in contrast with the Pd-catalyzed Heck aminocarbonylation used in the last step of Scheme 1.

To evaluate the SAR of these analogues for their AR antagonistic activities, ARE-luciferase reporter constructs were introduced into LNCaP prostate adenocarcinoma cancer cells that stably expressed either the WT AR (LNCaP AR cs) or the F877L mutant AR (LNCaP F877L) in a native AR setting.[28] The analogues **9**−**16** and **18**−**29** all acted as full antagonists in both cell lines and inhibited luciferase transcription with IC_{50} values ranging from 50 to >30 000 nM. Compounds **1** (enzalutamide) and **4** (JNJ-pan-AR) were used as controls (Table 2). No agonism of either AR F877L or the AR WT was

https://doi.org/10.1021/acsmedchemlett.1c00032
ACS Med. Chem. Lett. 2021, 12, 1245−1252

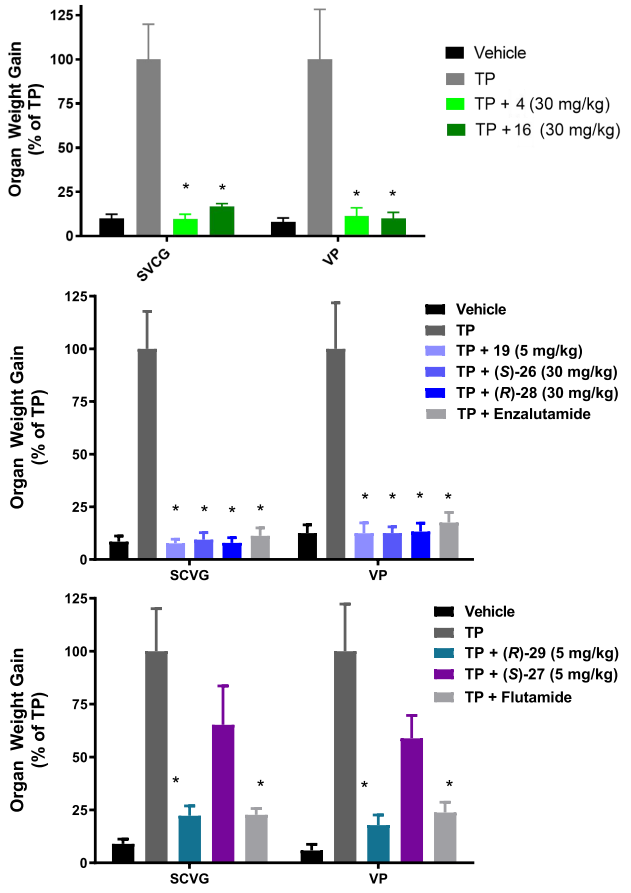

Figure 5. Hershberger assay: Dosing effect of compounds **16** (30 mg/kg), **19** (5 mg/kg), (*S*)-**26** (30 mg/kg), and (*R*)-**28** (30 mg/kg) compared with control group **1** (enzalutamide, 30 mg/kg) and (*R*)-**29** (5 mg/kg) and (*S*)-**27** (5 mg/kg) compared with control group flutamide (3 mg/kg) on ASOs. The ASO development of seminal vesicles and coagulating glands (SVCG) and the ventral prostate (VP) is shown. The compound-dependent suppression of ASOs is significant for each compound tested ($p \leq 0.0001$, *t*-test/Mann–Whitney). Data are the mean ± SD ($n = 6$).

observed for spirocyclic compounds under the assay conditions.

The unsubstituted (R_1 = H) analogues **9** (F877L IC_{50} > 15 000 nM; WT IC_{50} > 15 000 nM) and **10** (F877L IC_{50} = 5012 nM; WT IC_{50} = 11 220 nM) were at least 10 times less potent compared with the corresponding *N*-methylated (R_1 = Me) compounds **11** (F877L IC_{50} = 676 nM; WT IC_{50} = 1380 nM) and **12** (F877L IC_{50} = 525 nM; WT IC_{50} = 646 nM). However, the potencies of fluorinated (R_2 = F) **13** (F877L IC_{50} = 759 nM; WT IC_{50} = 1039 nM) and **14** (F877L IC_{50} = 339 nM; WT IC_{50} = 398 nM) were almost equal to or slightly better than those of nonfluorinated (R_2 = H) **11** and **12**. By contrast, hydantoin **15** (F877L IC_{50} = 1660 nM; WT IC_{50} = 5129 nM) lost significant potency compared with the corresponding thiohydantoin **12** (F877L IC_{50} = 525 nM; WT IC_{50} = 646 nM), confirming the importance of the thiocarbonyl moiety. It was notable that analogue **16** (F877L IC_{50} = 178 nM; WT IC_{50} = 219 nM) was a full antagonist and was almost equally potent as benchmark **4** (F877L IC_{50} = 98 nM; WT IC_{50} = 191 nM); both compounds possess a piperidinyloxy substituent on ring "B". A further potency increase was achieved in **18** (R_1 = i-Pr, F877L IC_{50} = 145 nM; WT IC_{50} = 112 nM), **19** (R_1 = i-Pr, F877L IC_{50} = 93 nM; WT IC_{50} = 93 nM), **20** (R_1 = i-Bu, F877L IC_{50} = 102 nM; WT IC_{50} = 100 nM), and **21** (R_1 = i-Bu, F877L IC_{50} = 123 nM; WT IC_{50} = 126 nM). An additional derivatization of R_1 in **22**–**25** did not further enhance the potency. Nevertheless, the potencies of **18**–**21** were comparable to or slightly better than that of **4**. Interestingly, chiral (*R*)-**28** (F877L IC_{50} = 65 nM; WT IC_{50} = 52 nM) and (*R*)-**29** (F877L IC_{50} = 78 nM; WT IC_{50} = 72 nM) were about two times more potent than the corresponding (*S*)-**26** (F877L IC_{50} = 112 nM; WT IC_{50} = 178 nM) and (*S*)-**27** (F877L IC_{50} = 151 nM; WT IC_{50} = 170 nM). The assignments of absolute stereochemistry for **26**–**29** were based on VCD experiments due to the unsuccessful efforts to obtain single crystals for X-ray studies and the inability to predict the potency difference in our homology model.[29,30] Significantly, these analogues remained full antagonists in both AR F877L and the AR WT despite having the same "B" substituents as **1** (enzalutamide) or **3** (apalutamide), both of which are agonists in AR F877L. This observation suggests the intrinsic propensity of scaffold **8** for antagonism against both AR F877L and the AR WT as well as for selectivity over the GR (Figure 4).[12]

To correlate the AR antagonism with an antiproliferative effect in androgen-dependent tumor cell lines, **12**, **16**, **18**–**20**, and **26**–**29** were also evaluated in a growth inhibition assay in the AR WT-dependent VCaP cells, again using **1** and **4** as comparators.[31] Luciferase transcription inhibition appeared to translate into antiproliferative activity in VCaP cells, tracking well with LNCaP WT potency with IC_{50} values ranging from 10 to 2440 nM (Table 3). The potencies of **16**, **18**–**20**, (*R*)-**28**, and (*R*)-**29** were comparable to or better than those of **1** and **4**.

In mouse single-dose pharmacokinetic (PK) studies, (*R*)-**29**, the more potent enantiomer of **19** (Table 1), displayed a higher area under the receiver operating characteristic (ROC) curve (AUC) (104 μg·h/mL) after oral dosing and lower clearance (CL 0.9 mL/min/kg) after IV dosing compared with the corresponding, less potent (*S*)-**27** (AUC 50.4 μg·h/mL, CL 3.0 mL/min/kg) (Table 3). The same trend was observed by comparing (*R*)-**28** and (*S*)-**26** in terms of the exposure and clearance, indicating the subtle difference between (*R*)- and (*S*)-enantiomers in terms of the PK characteristics. The overall PK parameters of (*R*)-**29** tracked well with its corresponding racemate, **19**. All analogues displayed favorable PK parameters, with oral bioavailability ranging from 61 to >100% (Table 4).

Compounds **16**, **19**, (*S*)-**26**, (*S*)-**27**, (*R*)-**28**, and (*R*)-**29** were evaluated in rats for their inhibitory effect on the growth of androgen-sensitive organs (ASOs) under stimulation by testosterone propionate (TP) in the Hershberger assay to assess their *in vivo* antiandrogen activities against the WT AR (Figure 5). Treatment with compounds **16**, (*S*)-**26**, and (*R*)-**28** resulted in statistically significant reductions in ASOs versus the TP control at 30 mg/kg once daily oral dosing for 10 days ($p > 0.0001$; Figure 5), comparable to that of positive control enzalutamide (**1**) at 30 mg/kg. Importantly, compound **19** showed a similar reduction in ASOs at 5 mg/kg. In a separate study, treatment with compound (*R*)-**29** resulted in statistically significant efficacy at 5 mg/kg once daily oral dosing for 10 days ($p \leq 0.0001$; Figure 5) compared with that of positive-control flutamide at 3 mg/kg. In contrast, compound (*S*)-**27** showed minimal effects on ASOs at 5 mg/kg (Figure 5), consistent with its less robust *in vitro* AR antagonistic potency (Tables 1 and 2) and lower *in vivo* PK exposure compared with (*R*)-**29** (Table 4).

https://doi.org/10.1021/acsmedchemlett.1c00032
ACS Med. Chem. Lett. 2021, 12, 1245–1252

Table 5. Incubation of 16, 17, and 50 in Dog Liver Microsomes with GSH in the Absence or Presence of NADPH[a]

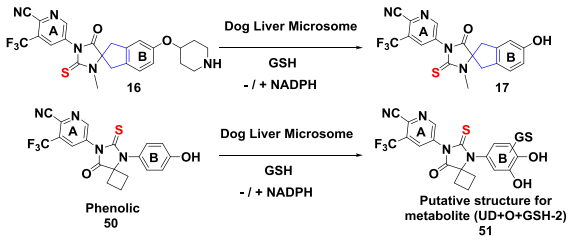

compound	50		17		16	
NADPH[b]	−	+	−	+	−	+
UD[c]	100.0%	78.7%	100.0%	52.3%	100.0%	98.4%
UD+O		9.2%		2.0%		0.19%
phenolic (**50** or **17**)[d]	NA	NA	NA	NA	0.01%	**1.4%**
UD+GSH-2H (a)				**10.7%**		**0.002%**[d]
UD+GSH-2H (b)				**1.8%**		
UD+O+GSH-2H		**12.1%**		**30.1%**		**0.01%**[d]
UD+O+GSH				**3.1%**		

[a]Final concentrations of the substrates (UD), dog liver microsomes, glutathione (GSH), and NADPH were 10 μM, 1 mg/mL, 5 mM, and 1 mM, respectively. The percent compositions of the parent drug and its metabolites were based on peak areas from 5 ppm accurate mass measurements with the assumption of equal positive electrospray ionizations. [b]−/+ means in the absence or in the presence of NADPH. [c]UD is defined as incubated substrate unchanged. [d]Phenolic refers to either metabolite **50** or **17**. [e]GSH conjugates detected from incubation with **16** were from metabolite **17**.

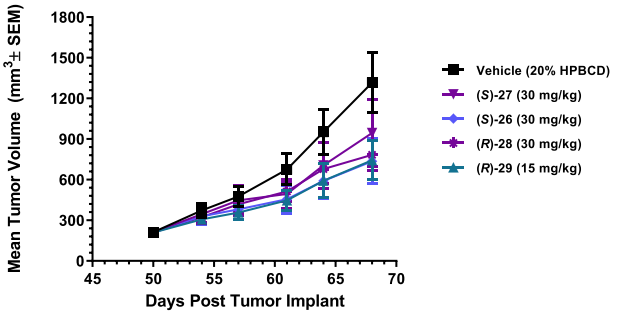

Figure 6. Oral *in vivo* efficacy profile of (*S*)-**26**, (*S*)-**27**, (*R*)-**28**, and (*R*)-**29** in castrated male SHO mice implanted with LNCaP F877L tumors cells. Tumors were measured twice weekly, and the results are presented as the average tumor volume, expressed as mm^3 ± the standard error of mean (SEM) of each group.

We previously reported the identification of phenolic derivative **50** (Table 5) as a key metabolite of compound **4** (JNJ-pan-AR, Figure 2). *In vitro* experiments demonstrated that **50** could be bioactivated in glutathione (GSH) trapping experiments, as indicated in Table 5, by the formation of GSH adducts such as the putative catechol structure **51**.[17] It is notable that the structural features in the periphery of ring "B" in compound **16** closely resemble those of compound **4** (JNJ-pan-AR), thus raising the possibility of similar bioactivation.[32] Like **4**, phenolic **17** was indeed detected in a small amount (1.4%) in trapping experiments together with a trace amount of two GSH adducts. The small amount of **17** reflected the low turnover of **16** under the *in vitro* assay conditions. Furthermore, phenolic **17** was moderately metabolized in the same experiments to generate at least four GSH adducts in significant amounts, including the two observed for **16**: UD +GSH-2H (10.7%) and UD+O+GSH-2H (30.1%). Presumably, one of the GSH adducts (UD+GSH-2H) was formed at the *para*-benzylic position of ring "B". These results suggested that compound **16** remained vulnerable to the bioactivation liability, and the next round of SAR iteration should investigate bioisosteric "B" rings such as pyridyl to mitigate potential bioactivation risks. We previously used a similar approach in the optimization of compound **4**, resulting in the successful identification of clinical stage compound **5** (JNJ-63576253).[17] However, such additional B-ring modifications in the spiro series are beyond the scope of this work.

Next, we tested the efficacy of compounds (*S*)-**26**, (*S*)-**27**, (*R*)-**28**, and (*R*)-**29** for their ability to suppress prostate tumor xenograft growth *in vivo*. Castrated male SHO mice bearing the established LNCaP AR F877L mutant-driven 3-D spheroid tumors were orally administered vehicle alone or compound (*S*)-**26**, (*S*)-**27**, (*R*)-**28**, or (*R*)-**29** at 15 or 30 mg/kg once daily for 18 days. As shown in Figure 6, the continuous administration of compound (*S*)-**26**, (*S*)-**27**, (*R*)-**28**, or (*R*)-**29** resulted in statistically significant tumor growth inhibition compared with the vehicle-treated control group: (*S*)-**26** (30 mg/kg, 58%, p = 0.0002), (*S*)-**27** (30 mg/kg, 32%, p = 0.0309), (*R*)-**28** (30 mg/kg, 46%, p = 0.0152), and (*R*)-**29** (15 mg/kg, 57%, p = 0.0008). Notably, compound (*R*)-**29** had similar efficacy as compound (*S*)-**26** but at half the dose (15 vs 30 mg/kg). This is likely a result of the improved *in vitro* potency of (*R*)-**29** combined with the lower *in vivo* clearance and the higher exposure. A minimal impact on body weight loss was observed, indicating that all compounds were well tolerated. Together, these *in vivo* data provide evidence that spirocyclic AR antagonist compounds not only inhibited the growth of ASOs but also demonstrated statistically significant *in vivo* activity against the mutant AR-driven tumor growth in this LNCaP AR F877L xenograft model.

In summary, we described the discovery of a new series of AR antagonists with a spirocyclic thiohydantoin core represented by scaffold **8**. SAR studies revealed the intrinsic propensity of this bioisoteric replacement of the core ring for full antagonism against both the wild-type and the F877L mutant AR. Our findings highlighted the advantage of this conformationally restricted spirocyclic thiohydantoin core to avoid reliance on peripheral functional groups to impart full antagonism of both the wild-type and the mutant AR. We also

https://doi.org/10.1021/acsmedchemlett.1c00032
ACS Med. Chem. Lett. 2021, 12, 1245−1252

described the favorable *in vitro* and *in vivo* pharmacological properties of (*R*)-**29** as a full antagonist against AR F877L. This result stands in sharp contrast with the antagonist-to-agonist switch observed with **1** (enzalutamide), despite (*R*)-**29** and **1** sharing almost identical structural features of peripheral rings "A" and "B". Although our hypothesis on the impact of conformational restriction on the antagonist-to-agonist switch appears to be valid within the series derived from scaffold **8**, we are unable to fully rationalize the mechanism of these antagonists at the molecular level. It will be useful to further validate our hypothesis using experimental approaches such as X-ray crystallography and nuclear magnetic resonance (NMR) in combination with molecular simulations. Nevertheless, the distinctive molecular architecture of scaffold **8** represents an appealing opportunity for the further exploration and development of next-generation AR pathway inhibitors.

■ ASSOCIATED CONTENT

Supporting Information

The Supporting Information is available free of charge at https://pubs.acs.org/doi/10.1021/acsmedchemlett.1c00032.

Assay and protocols: transcriptional reporter, proliferation, Hershberger, tumor xenograft efficacy, GSH screen for phenolic metabolites, detailed chemistry, VCD experiments, SFC traces, and modeling (PDF)

■ AUTHOR INFORMATION

Corresponding Authors

Zhuming Zhang − *Janssen Research and Development, Spring House, Pennsylvania 19477, United States;* orcid.org/0000-0002-5638-5320; Email: zzhang85@its.jnj.com

Gilles Bignan − *Janssen Research and Development, Spring House, Pennsylvania 19477, United States;* Email: gbignan@its.jnj.com

Authors

Peter J. Connolly − *Janssen Research and Development, Spring House, Pennsylvania 19477, United States*

Luis Trabalón Escolar − *Eurofins Villapharma, Murcia 30320, Spain*

Christian Rocaboy − *Eurofins Villapharma, Murcia 30320, Spain*

Vineet Pande − *Janssen Research and Development, B-2340 Beerse, Belgium*

Lieven Meerpoel − *Janssen Research and Development, B-2340 Beerse, Belgium*

Heng-Keang Lim − *Janssen Research and Development, Spring House, Pennsylvania 19477, United States*

Jonathan R. Branch − *Janssen Research and Development, Spring House, Pennsylvania 19477, United States;* orcid.org/0000-0003-4169-5753

Janine Ondrus − *Janssen Research and Development, Spring House, Pennsylvania 19477, United States*

Ian Hickson − *Janssen Research and Development, Spring House, Pennsylvania 19477, United States;* Present Address: I.H.: Cancer Research UK Newcastle Drug Discovery Unit, Newcastle University, Newcastle upon Tyne, United Kingdom.; orcid.org/0000-0002-9167-0514

Tammy L. Bush − *Janssen Research and Development, Spring House, Pennsylvania 19477, United States*

James R. Bischoff − *Janssen Research and Development, Spring House, Pennsylvania 19477, United States;* Present Address: J.R.B.: F. Hoffmann-La Roche Ltd., Molecular Targeted Therapies (Oncology), Basel, Switzerland.

Complete contact information is available at: https://pubs.acs.org/10.1021/acsmedchemlett.1c00032

Notes

The authors declare no competing financial interest.

■ ACKNOWLEDGMENTS

We thank Kathryn Packman (Janssen R&D, Cambridge, MA) and Leopoldo Luistro (Janssen R&D, Spring House, PA) for their contributions to the *in vivo* Hershberger and LNCaP AR F877L xenograft model studies; Samantha Allen (Janssen R&D, Spring House, PA) and Lori Westover (Janssen R&D, Spring House, PA) for their contributions to the transcriptional reporter assays; Bing Huang (Wuxi AppTec, Shanghai, China) and Christopher Teleha (Janssen R&D, Spring House, PA) for their contributions to the preparation and chiral SFC separation of the compounds described herein; and Jordan Nafie (BioTools, Jupiter, FL), Rina Dukor (BioTools, Jupiter, FL), and Ann Vos (Janssen R&D, Beerse, Belgium) for VCD experiments.

■ REFERENCES

(1) Quigley, D. A.; Dang, H. X.; Zhao, S. G.; Lloyd, P.; Aggarwal, R.; Alumkal, J. J.; Foye, A.; Kothari, V.; Perry, M. D.; Bailey, A. M.; Playdle, D.; Barnard, T. J.; Zhang, L.; Zhang, J.; Youngren, J. F.; Cieslik, M. P.; Parolia, A.; Beer, T. M.; Thomas, G.; Chi, K. N.; Gleave, M.; Lack, N. A.; Zoubeidi, A.; Reiter, R. E.; Rettig, M. B.; Witte, O.; Ryan, C. J.; Fong, L.; Kim, W.; Friedlander, T.; Chou, J.; Li, H.; Das, R.; Li, H.; Moussavi-Baygi, R.; Goodarzi, H.; Gilbert, L. A.; Lara, P. N., Jr.; Evans, C. P.; Goldstein, T. C.; Stuart, J. M.; Tomlins, S. A.; Spratt, D. E.; Cheetham, R. K.; Cheng, D. T.; Farh, K.; Gehring, J. S.; Hakenberg, J.; Liao, A.; Febbo, P. G.; Shon, J.; Sickler, B.; Batzoglou, S.; Knudsen, K. E.; He, H. H.; Huang, J.; Wyatt, A. W.; Dehm, S. M.; Ashworth, A.; Chinnaiyan, A. M.; Maher, C. A.; Small, E. J.; Feng, F. Y. Genomic hallmarks and structural variation in metastatic prostate cancer. *Cell* **2018**, *174* (3), 758−769.

(2) Fujita, K.; Nonomura, N. Role of Androgen Receptor in Prostate Cancer: A Review. *World J. Mens Health.* **2019**, *37* (3), 288−295.

(3) De Bono, J. S.; Logothetis, C. J.; Molina, A.; Fizazi, K.; North, S.; Chu, L.; Chi, K. N.; Jones, R. J.; Goodman, O. B., Jr.; Saad, F.; Staffurth, J. N.; Mainwaring, P.; Harland, S.; Flaig, T. W.; Hutson, T. E.; Cheng, T.; Patterson, H.; Hainsworth, J. D.; Ryan, C. J.; Sternberg, C. N.; Ellard, S. L.; Fléchon, A.; Saleh, M.; Scholz, M.; Efstathiou, E.; Zivi, A.; Bianchini, D.; Loriot, Y.; Chieffo, N.; Kheoh, T.; Haqq, C. M.; Scher, H. I. Abiraterone and increased survival in metastatic prostate cancer. *N. Engl. J. Med.* **2011**, *364* (21), 1995−2005.

(4) Scher, H. I.; Fizazi, K.; Saad, F.; Taplin, M. E.; Sternberg, C. N.; Miller, K.; de Wit, R.; Mulders, P.; Chi, K. N.; Shore, N. D.; Armstrong, A. J.; Flaig, T. W.; Fléchon, A.; Mainwaring, P.; Fleming, M.; Hainsworth, J. D.; Hirmand, M.; Selby, B.; Seely, L.; de Bono, J. S. Increased survival with enzalutamide in prostate cancer after chemotherapy. *N. Engl. J. Med.* **2012**, *367* (13), 1187−1197.

(5) Smith, M. R.; Saad, F.; Chowdhury, S.; Oudard, S.; Hadaschik, B. A.; Graff, J. N.; Olmos, D.; Mainwaring, P. N.; Lee, J. Y.; Uemura, H.; Lopez-Gitlitz, A.; Trudel, G. C.; Espina, B. M.; Shu, Y.; Park, Y. C.; Rackoff, W. R.; Yu, M. K.; Small, E. J. Apalutamide treatment and metastasis-free survival in prostate cancer. *N. Engl. J. Med.* **2018**, *378* (15), 1408−1418.

(6) Schweizer, M. T.; Yu, E. Y. Persistent androgen receptor addiction in castration-resistant prostate cancer. *J. Hematol. Oncol.* **2015**, *8*, 128.

(7) Viswanathan, S. R.; Ha, G.; Hoff, A. M.; Wala, J. A.; Carrot-Zhang, J.; Whelan, C. W.; Haradhvala, N. J.; Freeman, S. S.; Reed, S. C.; Rhoades, J.; Polak, P.; Cipicchio, M.; Wankowicz, S. A.; Wong, A.; Kamath, T.; Zhang, Z.; Gydush, G. J.; Rotem, D.; et al. Structural alterations driving castration-resistant prostate cancer revealed by linked-read genome sequencing. *Cell* **2018**, *174* (2), 433−447.
(8) Robinson, D.; Van Allen, E. M.; Wu, Y. M.; Schultz, N.; Lonigro, R. J.; Mosquera, J. M.; Montgomery, B.; Taplin, M. E.; Pritchard, C. C.; Attard, G.; Beltran, H.; Abida, W.; Bradley, R. K.; Vinson, J.; Cao, X.; Vats, P.; Kunju, L. P.; Hussain, M.; Feng, F. Y.; Tomlins, S. A.; Cooney, K. A.; Smith, D. C.; Brennan, C.; Siddiqui, J.; Mehra, R.; Chen, Y.; Rathkopf, D. E.; Morris, M. J.; Solomon, S. B.; Durack, J. C.; Reuter, V. E.; Gopalan, A.; Gao, J.; Loda, M.; Lis, R. T.; Bowden, M.; Balk, S. P.; Gaviola, G.; Sougnez, C.; Gupta, M.; Yu, E. Y.; Mostaghel, E. A.; Cheng, H. H.; Mulcahy, H.; True, L. D.; Plymate, S. R.; Dvinge, H.; Ferraldeschi, R.; Flohr, P.; Miranda, S.; Zafeiriou, Z.; Tunariu, N.; Mateo, J.; Perez-Lopez, R.; Demichelis, F.; Robinson, B. D.; Schiffman, M.; Nanus, D. M.; Tagawa, S. T.; Sigaras, A.; Eng, K. W.; Elemento, O.; Sboner, A.; Heath, E. I.; Scher, H. I.; Pienta, K. J.; Kantoff, P.; de Bono, J. S.; Rubin, M. A.; Nelson, P. S.; Garraway, L. A.; Sawyers, C. L.; Chinnaiyan, A. M. Integrative clinical genomics of advanced prostate cancer. *Cell* **2015**, *161* (5), 1215−1228.
(9) Antonarakis, E. S.; Lu, C.; Wang, H.; Luber, B.; Nakazawa, M.; Roeser, J. C.; Chen, Y.; Mohammad, T. A.; Chen, Y.; Fedor, H. L.; Lotan, T. L.; Zheng, Q.; De Marzo, A. M.; Isaacs, J. T.; Isaacs, W. B.; Nadal, R.; Paller, C. J.; Denmeade, S. R.; Carducci, M. A.; Eisenberger, M. A.; Luo, J. AR-V7 and resistance to enzalutamide and abiraterone in prostate cancer. *N. Engl. J. Med.* **2014**, *371* (11), 1028−1038.
(10) Joseph, J. D.; Lu, N.; Qian, J.; Sensintaffar, J.; Shao, G.; Brigham, D.; Moon, M.; Maneval, E. C.; Chen, I.; Darimont, B.; Hager, J. H. A clinically relevant androgen receptor mutation confers resistance to second-generation antiandrogens enzalutamide and ARN-509. *Cancer Discovery* **2013**, *3* (9), 1020−1029.
(11) Korpal, M.; Korn, J. M.; Gao, X.; Rakiec, D. P.; Ruddy, D. A.; Doshi, S.; Yuan, J.; Kovats, S. G.; Kim, S.; Cooke, V. G.; Monahan, J. E.; Stegmeier, F.; Roberts, T. M.; Sellers, W. R.; Zhou, W.; Zhu, P. An F876L mutation in androgen receptor confers genetic and phenotypic resistance to MDV3100 (enzalutamide). *Cancer Discovery* **2013**, *3* (9), 1030−1043.
(12) Arora, V. K.; Schenkein, E.; Murali, R.; Subudhi, S. K.; Wongvipat, J.; Balbas, M. D.; Shah, N.; Cai, L.; Efstathiou, E.; Logothetis, C.; Zheng, D.; Sawyers, C. L. Glucocorticoid receptor confers resistance to antiandrogens by bypassing androgen receptor blockade. *Cell* **2013**, *155* (6), 1309−1322.
(13) Nelson, P. S. Targeting the androgen receptor in prostate cancer–a resilient foe. *N. Engl. J. Med.* **2014**, *371* (11), 1067−1069.
(14) Tan, M. H.; Li, J.; Xu, H. E.; Melcher, K.; Yong, E. L. Androgen receptor: structure, role in prostate cancer and drug discovery. *Acta Pharmacol. Sin.* **2015**, *36* (1), 3−23.
(15) Rathkopf, D. E.; Smith, M. R.; Ryan, C. J.; Berry, W. R.; Shore, N. D.; Liu, G.; Higano, C. S.; Alumkal, J. J.; Hauke, R.; Tutrone, R. F.; Saleh, M.; Chow Maneval, E.; Thomas, S.; Ricci, D. S.; Yu, M. K.; de Boer, C. J.; Trinh, A.; Kheoh, T.; Bandekar, R.; Scher, H. I.; Antonarakis, E. S. Androgen receptor mutations in patients with castration-resistant prostate cancer treated with apalutamide. *Ann. Oncol.* **2017**, *28* (9), 2264−2271.
(16) Moilanen, A. M.; Riikonen, R.; Oksala, R.; Ravanti, L.; Aho, E.; Wohlfahrt, G.; Nykänen, P. S.; Törmäkangas, O. P.; Palvimo, J. J.; Kallio, P. J. Discovery of ODM-201, a new-generation androgen receptor inhibitor targeting resistance mechanisms to androgen signaling-directed prostate cancer therapies. *Sci. Rep.* **2015**, *5*, 12007.
(17) Zhang, Z.; Connolly, P. J.; Lim, H. K.; Pande, V.; Meerpoel, L.; Teleha, C.; Branch, J. R.; Ondrus, J.; Hickson, I.; Bush, T.; Luistro, L.; Packman, K.; Bischoff, J. R.; Ibrahim, S.; Parrett, C.; Chong, Y.; Gottardis, M. M.; Bignan, G. Discovery of JNJ-63576253: a clinical stage androgen receptor antagonist for F877L mutant and wild-type castration resistant prostate cancer (mCRPC). *J. Med. Chem.* **2021**, *64* (2), 909−924.
(18) Liu, H.; Han, R.; Li, J.; Liu, H.; Zheng, L. Molecular mechanism of R-bicalutamide switching from androgen receptor antagonist to agonist induced by amino acid mutations using molecular dynamics simulations and free energy calculation. *J. Comput.-Aided Mol. Des.* **2016**, *30* (12), 1189−1200.
(19) Liu, H. L.; Zhong, H. Y.; Song, T. Q.; Li, J. Z. A Molecular Modeling Study of the Hydroxyflutamide resistance mechanism induced by androgen receptor Mutations. *Int. J. Mol. Sci.* **2017**, *18* (9), No. 1823.
(20) Liu, H.; Wang, L.; Tian, J.; Li, J.; Liu, H. Molecular Dynamics Studies on the enzalutamide resistance mechanisms induced by androgen receptor mutations. *J. Cell. Biochem.* **2017**, *118* (9), 2792−2801.
(21) Jung, M. E.; Ouk, S.; Yoo, D.; Sawyers, C. L.; Chen, C.; Tran, C.; Wongvipat, J. Structure−activity relationship for thiohydantoin androgen receptor antagonists for castration-resistant prostate cancer (CRPC). *J. Med. Chem.* **2010**, *53* (7), 2779−2796.
(22) Soengas, R. G.; Silva, S. Spirocyclic nucleosides in medicinal chemistry: an overview. *Mini-Rev. Med. Chem.* **2012**, *12* (14), 1485−1496.
(23) Balbas, M. D.; Evans, M. J.; Hosfield, D. J.; Wongvipat, J.; Arora, V. K.; Watson, P. A.; Chen, Y.; Greene, G. L.; Shen, Y.; Sawyers, C. L. Overcoming mutation-based resistance to antiandrogens with rational drug design. *eLife* **2013**, *2*, No. e00499.
(24) Wang, A.; Wang, Y.; Meng, X.; Yang, Y. Design, synthesis and biological evaluation of novel thiohydantoin derivatives as potent androgen receptor antagonists for the treatment of prostate cancer. *Bioorg. Med. Chem.* **2021**, *31*, 115953.
(25) Murigi, F. N.; Nichol, G. S.; Mash, E. A. Synthesis of the conformationally constrained tyrosine analogues, (R)- and (S)-5-hydroxy-2-aminoindan-2-carboxylic acids. *J. Org. Chem.* **2010**, *75* (4), 1293−1296.
(26) Kotha, S.; Brahmachary, E. Synthesis of indan-based unusual α-amino acid derivatives under phase-transfer catalysis conditions. *J. Org. Chem.* **2000**, *65* (5), 1359−1365.
(27) Więckowska, A.; Fransson, R.; Odell, L. R.; Larhed, M. Microwave-assisted synthesis of Weinreb and MAP aryl amides via Pd-catalyzed Heck aminocarbonylation using $Mo(CO)_6$ or $W(CO)_6$. *J. Org. Chem.* **2011**, *76* (3), 978−981.
(28) Chen, C. D.; Welsbie, D. S.; Tran, C.; Baek, S. H.; Chen, R.; Vessella, R.; Rosenfeld, M. G.; Sawyers, C. L. Molecular determinants of resistance to antiandrogen therapy. *Nat. Med.* **2004**, *10* (1), 33−39.
(29) Böselt, L.; Sidler, D.; Kittelmann, T.; Stohner, J.; Zindel, D.; Wagner, T.; Riniker, S. Determination of Absolute Stereochemistry of Flexible Molecules Using a Vibrational circular dichroism spectra alignment algorithm. *J. Chem. Inf. Model.* **2019**, *59* (5), 1826−1838.
(30) Stephens, P. J.; Devlin, F. J.; Pan, J. J. The determination of the absolute configurations of chiral molecules using vibrational circular dichroism (VCD) spectroscopy. *Chirality* **2008**, *20* (5), 643−63.
(31) Korenchuk, S.; Lehr, J. E.; Mclean, L.; Lee, Y. G.; Whitney, S.; Vessella, R.; Lin, D. L.; Pienta, K. J. VCaP, a cell-based model system of human prostate cancer. *In Vivo* **2001**, *15* (2), 163−168.
(32) Naven, R. T.; Swiss, R.; Klug-McLeod, J.; Will, Y.; Greene, N. The development of structure-activity relationships for mitochondrial dysfunction: uncoupling of oxidative phosphorylation. *Toxicol. Sci.* **2013**, *131* (1), 271−278.

https://doi.org/10.1021/acsmedchemlett.1c00032
ACS Med. Chem. Lett. 2021, 12, 1245−1252